Anisotropic fluid diffusion in carbon fiber reinforced composite rods: Experimental, analytical and numerical study

Abedin Gagani* [(a)], Andrejs Krauklis [(a)], Andreas T. Echtermeyer [(a)]

[(a)] Department of Mechanical and Industrial Engineering, Norwegian University of Science and Technology, Richard Birkelandsvei 2b, Trondheim, Norway

Abstract

Carbon fiber composite plastic (CFRP) rods immersed in water present a pronounced anisotropic diffusion behavior. Understanding and predicting this behavior is important as the mechanical properties of the material are influenced by the moisture content. A simple experimental procedure allowing identification of both radial and axial diffusivity is presented. The diffusivities are calculated based on a new anisotropic analytical or numerical analysis. The diffusivity in the axial direction was found to be 14.3 times the diffusivity in radial direction. The analytical and numerical approach show a good agreement. A practical engineering case study is also presented: the moisture content profile of a carbon fiber rod inside a cylindrical metal end fitting for long exposure times (5, 10, 25 and 50 years).

Keywords: Environmental degradation composites; Fluid diffusion composites; Analytical diffusion composites, FE diffusion composites; Diffusion composite cylinders

* Corresponding author
E-mail: abedin.gagani@ntnu.no (A.Gagani)

1. Introduction

Composite materials for structural components are often used in humid environments. Typical examples are marine, offshore and aircraft structures. For marine environments, composites have an interesting potential, due to their light-weight combined with high stiffness, strength and excellent corrosion resistance. Deep-water applications of composites, such as risers and tethers have been considered and a composite riser joint is currently in operation [1-3]. Thermoplastic Composites Pipes are currently used for intervention and injection lines, but they are also considered for risers [4-7]. Composite tethers are elements that constrain tension leg platforms (TLPs) to the seafloor, **Fig.1**. The load carrying elements of a tether are several strands of carbon fiber reinforced plastic (CFRP) rods. The design of the tethers is based on the platform natural frequency [3]; they need to be very stiff, strong and lightweight. CFRP rods have not been used as tethers for platforms yet, but the same technology has been used to stiffen and support deep-water umbilicals [8]. Umbililicas are combined hydraulic and electrical lines going from a platform to the sea bead, providing power for subsea components. CFRP are also considered for supporting bridges and cables.

During service life, CFRP in marine applications are constantly immersed in water. Structural assessment of the CFRP is performed using both dry and degraded mechanical strength [9]. Material properties are obtained experimentally testing dry and saturated wet samples. For the choice of the correct material properties, it is necessary to know if a section of the composite structure is still dry after years of water exposure or degraded due to water having diffused into the material.

Fig.1 Scheme of a tension leg platform (TLP)

Fluid diffusion in composites has been studied since the early works collected by Springer [10, 11]. In these early contributions, it was already clear that the diffusivity of composite materials is not isotropic, due to their heterogeneous structure. More recent studies performed on this topic used commercial FE software due to the availability of mass diffusion analyses in the programs [12]. Nevertheless, very few studies about water diffusion in composite rods have been presented. Barjasteh and Nutt [13], studied water diffusion in unidirectional hybrid rods, having Carbon Fiber CF-Epoxy in the internal part and Glass Fiber GF-Epoxy in the external part; measuring weight gain curves of both end-capped and uncapped sampled with the same geometry. They reported an axial diffusivity almost 5 times higher than the radial diffusivity for CF-Epoxy rods, 3 times higher than the radial diffusivity for GF-Epoxy rods and 4 times higher than the radial diffusivity for hybrid CF/GF-Epoxy rods. This effect is attributed to the more torturous path that water diffusing in the direction transverse to the fibers follows, compared to water diffusing along the fiber direction. However, it has been suggested that also the fiber-matrix interphase plays a significant role in water diffusion in composites [14]. Recent works of Joliff et al. [15, 16], based on microthermal analyses and atomic force measurements (AFM), have shown that the fiber-matrix interphase has a higher diffusivity than the bulk matrix, due to the less dense crosslinking and local plasticization [17].

Recent works have been published about FE micromechanical modelling of composites with high diffusivity interphases implemented [15, 16, 18, 19]. Rocha et al. [18], simulated anisotropic diffusion in GF-Epoxy composite plates modelling a high diffusivity fibre-matrix interphase. The importance of these models is the fact that they can enable prediction of anisotropic diffusivity starting from the diffusivitiy of the constituents: matrix, fibres and interphase.

From a practical application point of view, one of the drawbacks of micromechanical models is their complexity and lack of direct experimental measurements of the constituent properties, especially the fiber-matrix interphase diffusivity.

Based on these limitations, an analytical and numerical homogeneous anisotropic diffusion model is employed here for composite rods. This model can predict the anisotropic nature of diffusion in composites, overcoming the experimental and modeling complications that microscale strategies would introduce.

The identification of anisotropic diffusivity is not a trivial task, especially when dealing with non-flat structures, as rods or pipes, where it is difficult to create conditions for unidirectional mass flow. For long rods, the contribution of diffusion through the cylindrical surfaces will dominate, leading to a nearly pure radial diffusion. For gradually shorter rods, the contribution of diffusion in the axial direction becomes larger.

This characteristic can be used to compute axial and radial diffusivity.

By measuring the weight gain of immersed samples with different lengths it is possible to identify both radial and axial diffusivity. This provides a powerful tool for the prediction of water uptake in CFRP rods.

Finally, a case study of industrial interest is presented: the prediction of water diffusion in a carbon fiber composite tether end-fitting filled with epoxy after 5, 10, 25 and 50 years of water exposure. This case study is analyzed using a homogeneous anisotropic FE model.

2. Experimental measurements

2.1. Materials

The Carbon Fiber Reinforced Plastic CFRP rods tested in this work are 6 mm pultruded rods (average fiber radius 2.97 ± 0.44 μm) and vinylester resin. Fiber volume fraction, measured by means of microscope analysis, was 50 % ± 2 % respectively. More information about the materials and the mechanical properties are available in [3, 20]. All samples were cut using a water-cooled diamond saw. They were cut to six different lengths: 3, 6, 30, 60, 180 and 300 mm. These lengths were adopted to investigate the difference between mainly axial diffusion and mainly radial diffusion. The samples are shown in **Fig.2**.

For each geometry, three samples were prepared.

Ramirez et al. [21] reported that in carbon fiber vinylester composites, fluid diffusion causes degradation of the fiber-matrix interphase, which can contain more moisture than the bulk matrix. For carbon fiber vinylester, it was reported that the interphase accounts for 90% of the water totally absorbed by the composites [21]. The degraded fiber-matrix interphase can act as a high diffusivity path being the main reason behind the pronounced anisotropic behavior of the composite. Optical micrographs in **Fig.3** and **Fig.4** show a comparison of dry and conditioned samples. From the optical micrographs, it is possible to notice a 0.4 - 1 μm thick interphase around each fiber for the samples saturated with water (degraded).

Fig.2 Tested CFRP rods. The diameter is 6 mm the lengths are 3, 6, 30, 60, 180 and 300 mm

Fig.3 (a) Optical micrographs of dry CFRP pultruded rod. There is no visible damage in the interphase between matrix and fibers. (b) Optical micrographs of conditioned CFRP pultruded rod. Extensive damage is visible in the interphase between matrix and fibers

Fig.4 High magnification optical micrographs of dry and conditioned CFRP pultruded rod. Degradation in the 0.4 - 1 μm thick fiber-matrix interphase is visible

2.2. Water uptake measurements

Initially, samples were dried in an oven at 40˚C and their weight was recorded until stabilization occurred. Subsequently a conditioning chamber was prepared by filling a thermally insulated bucket with distilled water. An electrical resistance was installed inside the bucket for heating up the water. A thermocouple was placed in the bucket in order to measure water temperature and regulate the heat emitted by the electrical resistance. The ASTM standard D5229 [22] recommends choice of conditioning temperature at least 25°C below the glass transition temperature of the polymer matrix. For vinyl ester the glass transition temperature is between 115°C and 155°C [21, 23]. Based on this consideration, a temperature of 60˚C ± 1 ˚C was adopted here. This temperature provides a convenient acceleration of the test without activating additional mechanisms that could influence the water uptake process, [24]. Water was changed regularly in order to simulate the conditions of a material immersed in an infinitely big water bath, and avoiding potential degradation products from influencing the diffusion process. A U-shaped aluminum holder was used to maintain the samples in position and to avoid contact between them, guarantying exposure to water for almost the entire surface of the samples. The samples were intentionally not coated, in order to capture the effect of the material anisotropy.

Weight gain measurements were performed according to the ASTM Standard D5229 [22]. The samples were extracted from the conditioning chamber, they were dried with a cloth and they were weighted using a Mettler Toledo AG204 DeltaRange scale, having a sensitivity of 0,1 mg and a capacity of 61 g. The samples ‘weight was recorded and the weight increase was calculated according to the standard [22] as follows:

$$w(t) = 100 \cdot \frac{m(t)}{m_i} \quad (1)$$

where m_i is the initial dry mass, $m(t)$ the recorded mass and $w(t)$ the percentage mass increase.

3. Analytical diffusion model

The analytical anisotropic diffusion model presented here is based on Fick's second law [25]. For an infinitely long cylindrical isotropic material diffusion is governed by the following equation [26]:

$$\frac{\partial c}{\partial t} = \frac{1}{r}\frac{\partial}{\partial r}\left(r D_R \frac{\partial c}{\partial r}\right) \quad (2)$$

where $c(r,t)$ is the moisture content, D_R is the radial diffusivity and r is the radial coordinate, according to the reference system in **Fig.5**.

The solution of Eq. (2) is given in [26]:

$$c(r,t) = c_\infty \left(1 - 2\sum_{n=1}^{\infty} \frac{\exp\left(-\frac{D_R \alpha_n^2 t}{R^2}\right) J_0\left(\frac{r\alpha_n}{R}\right)}{\alpha_n J_1(\alpha_n)}\right) \quad (3)$$

where R is the radius of the cylinder, c_∞ is the saturation moisture content, J_0 the Bessel function of order zero, J_1 the Bessel funtion of first order and α_n the roots of Eq. (4):

$$J_0(\alpha_n) = 0 \quad (4)$$

Integration of Eq. (3) over the cylinder's volume provides the moisture content within the whole specimen [26]:

$$M(t) = 2L\int_0^R 2\pi r\, c(r,t)\, dr \quad (5)$$

$$M(t) = M_\infty \left[1 - \sum_{n=1}^{\infty} \frac{4}{(\alpha_n)^2} \exp\left(-\frac{\alpha_n^2 D_R t}{R^2}\right)\right] \quad (6)$$

where M(t) is the amount of moisture in the whole cylinder and M_∞ the saturation moisture content in the whole cylinder.

For a particular case of anisotropic materials: axial symmetric orthotropic materials, Fick's diffusion second law in cylindrical coordinates becomes [13]:

$$\frac{\partial c}{\partial t} = D_Z \frac{\partial^2 c}{\partial z^2} + D_R \frac{1}{r} \frac{\partial}{\partial r}\left(r \frac{\partial c}{\partial r}\right) \quad (7)$$

where z is the axial coordinate, as shown in **Fig.5**. In Eq. (7). The azimuthal term (φ) of the diffusion equation is not present, due to symmetry considerations. Axial symmetry conditions are assumed.

Fig.5 Cylindrical coordinate system and dimensions for anisotropic cylinders

The general analytical solution of this problem is reported by Watson et al. in [27].

The boundary conditions (BC) that need to be imposed for the case of an initially dry cylinder immersed in water are:

$$c(r, z, t = 0) = 0 \quad (8)$$

$$c(R, z, t > 0) = c_\infty \quad (9)$$

$$c(r, \pm L, t > 0) = c_\infty \quad (10)$$

The BC in Eq. (8) imposes an initially dry sample, while the BCs in Eq. (9) and Eq. (10) impose fluid exposure on the cylindrical and end surfaces of the cylinder respectively.

Employing the BCs in Eq. (8), Eq. (9) and Eq. (10) in the general solution reported by Watson et al. [27], it is possible to obtain the moisture content in the cylinder:

$$M(t) = \int_{-L}^{L} dz \cdot \int_{0}^{R} 2\,\pi\, r\, c(r,t)\, dr \tag{11}$$

$$M(t) = M_\infty \left[1 - 4 \sum_{m=1}^{\infty} \frac{1}{(\alpha_m)^2} \exp\left(\frac{-\alpha_m^2 D_R\, t}{R^2}\right) \cdot \frac{8}{\pi^2} \sum_{n=0}^{\infty} \frac{1}{(2n+1)^2} \exp\left(-\frac{(2n+1)^2 \pi^2}{4L^2} D_Z t\right)\right] \tag{12}$$

where L is the half length of the cylinder, D_R the radial diffusivity, D_Z the axial diffusivity and α_m the roots of Bessel function of order zero: $J_0(\alpha_m) = 0$. Eq. (12) was implemented using m = 25 and n = 25.

Eq. (6) is valid for purely radial diffusion. This condition is encountered experimentally only for infinitely long rods or for rods where moisture ingress through the edges is impeded by caps or coating. Eq. (12) describes diffusion in rods of arbitrary length having different diffusivities in axial and radial direction, hence anisotropic rods. However, Eq. (12) can also be used for analysis of rods of arbitrary length having an isotropic diffusivity, using $D_Z = D_R$. Eq. (12) for radial and axial diffusion in an anisotropic material was obtained for a cylinder under the boundary conditions in Eqs. (8-10). Different geometries, or boundary conditions (BCs), would result in a different analytical solution; which could become difficult to derive for most engineering applications. In order to provide a more flexible tool in case of arbitrary geometry and BCs, a finite element model (FE) is introduced below. The results of the FE model are reported together with the results of the analytical model and compared to the experimental results. Furthermore, the FE model is used for the analysis of a case study, a composite rod terminated in a metal end fitting.

4. Numerical diffusion model

A parametric finite element study was performed using ABAQUS ™. Fickian mass diffusion analysis was performed using an axisymmetrical model. DCAX4 elements were adopted: 4-node linear axisymmetric heat transfer quadrilateral element, having the size 0.1 mm x 0.1 mm. This element size was chosen after a numerical convergence study.

Four material constants are required for the analysis: initial moisture content c_0, saturation moisture content c_∞, moisture diffusivity in the radial direction D_R and moisture diffusivity in the axial directon D_Z.

The procedure used for obtaining the radial and axial diffusivity from the experiments is reported and discussed in more detail in the next paragraph. A mass diffusion step was used in the FE analysis; the initial boundary condition was set as zero moisture content in the whole model. The boundary condition in the analysis step was set as water exposure in all the outer surfaces of the rod. The boundary conditions are shown in **Fig. 6**, where arrows indicate the surfaces exposed to water.

It is worth noticing that the boundary conditions used in the FE model are the same as the ones used for the analytical model, presented in the previous Paragraph. They represent water exposure on all the external surfaces of an axisymmetric cylindrical sample.

Fig.6 Coordinate system, dimensions and mesh adopted for the 6 mm long rod FE model. Arrows indicate the surfaces exposed to water. Coordinate system and boundary conditions ‘equations are also reported.

5. Results and Discussion

Weight gain measurements are reported in **Fig.7**. All samples have 6 mm diameter and the following lengths: 3, 6 , 30 , 60 , 180 and 300 mm. The results are plotted as percentual weight gain versus square root of time, as in most of the technical literature [10, 11].

A near linear behaviour up to 1600 hours of exposure is observed. For short samples, higher scatter is present in the measurement, due to higher incidence of the scale sensibility on the mass measurement.

The smallest 3 mm long samples reached saturation within the measurement period. The other samples were too large to be fully saturated. Based on the 3 mm long samples the saturation level of mass increase due to water was found to be 1.4% ± 0.29 %.

Fig.7 Weight gain curves for the conditioned samples compared with analytical and FE results obtained using anisotropic diffusivity

5.1. Identification of the diffusion constants based on the analytical model

The measured water uptake is a combination of radial and axial diffusion. In principle, measurements on two geometries should be sufficient for obtaining D_R and D_Z. Six different geometries were tested in order to explore the range between purely radial diffusion and radial-axial diffusion.

The flowchart in **Fig. 8** shows the steps necessary to identify the radial and the axial diffusivities: D_R and D_Z respectively.

Fig.8 Flowchart for the identification of radial and axial diffusivity

The first step is assuming that for long rods only radial diffusion is dominant, while axial diffusion can be neglected.

For long rods (L = 300 and L = 180 mm), nonlinear regression between the experimental measurements and the radial diffusion equation, Eq. (6), was performed, obtaining the best fit for $D_R = 4.81 \cdot 10^{-8}$ mm^2/s. The regression method adopted was nonlinear Generalized Reduced Gradient (GRG nonlinear) algorithm, which was performed minimizing the residual sum of squares.

The value of axial diffusion was then obtained by setting the value of radial diffusion to the newly obtained value ($D_R = 4.81 \cdot 10^{-8}$ mm^2/s) and performing GRG nonlinear regression between the experimental measurements for the 6 mm long rods and Eq. (12), describing both radial and axial diffusion. The regression was not based on the 3 mm long rods due to the higher scatter that these measurements present. The result was $D_Z = 6.90 \cdot 10^{-7}$ mm^2/s, hence a 14.3 times higher axial diffusivity than radial diffusivity. Coefficients of determination between experimental results and analytical results using obtained radial diffusivity ($D_R = 4.81 \cdot 10^{-8}$ mm^2/s) and axial diffusivity ($D_Z = 6.90 \cdot 10^{-7}$ mm^2/s) for rods of different length are reported in **Table 1**. Results of the regression analysis indicate, that for rods longer or equal to 180 mm, axial diffusivity can be neglected, thus simplifying the problem to radial diffusion only. For rods of length smaller or equal to 30 mm, both axial and radial diffusivity are significant.

Table1: Coefficients of determination describing the quality of the model calculations.

Experimental measurements and anisotropic diffusion analytical results, adopting D_R = 4.81 10^{-8} mm^2/s and D_Z = 6.90 10^{-7} mm^2/s, are shown in **Fig.7**.

The anisotropic diffusion model shows good agreement with experimental results in a wide range of rod lengths, whereas the isotropic diffusion model fails to predict diffusion in short rods, **Fig. 9**. Diffusion anisotropy is an inherent characteristic for composite rods, caused by the non-homogeneity of the material. For short composite rods the contribution of axial diffusivity is important, therefore only an anisotropic diffusion model can correctly predict the weight gain of the sample, while an isotropic model fails to correctly predict water uptake.

The diffusivity obtained experimentally is also comparable to results obtained by Figliolini and Carlsson [28], that measured values between 1.47 10^{-7} mm^2/s and 8.52 10^{-7} mm^2/s for CF vinylester samples obtained by vacuum-assisted resin transfer molding (VARTM) and exposed to 40°C seawater.

In both **Figs. 7** and **9** it can be observed that weight gain curves for 300, 180, 60 and 30 mm rods have quite small dispersion, while 6 and 3 mm long rods have higher dispersion. The higher dispersion of weight gain measurements for short rods is caused by the reduced scale sensitivity compared to the samples' mass.

5.2. Identification of the diffusion constants based on the FE model

The FE model was employed to predict the mass increase of the samples with time, based on the diffusivities D_R and D_Z. The best choice of diffusivities can be found by an iterative process, in an analogous way as described for the analytical model. As expected, the process gave the same constants as found from the analytical model. The predictive curves from the

FE model are also shown in **Fig. 8**. The difference between the FE and analytical curves is minimal.

The small deviation observed between analytical and FE results for short conditioning times is due to the fact that numerical simulations typically solve diffusion problems by means of series of error functions, which are very suitable for numerical evaluation at small intervals. The analytical solution for cylindrical problems, on the other hand, is based on series of Bessel functions, which converge better for long evaluation times. A more detailed discussion of these aspects is given by Crank [26].

5.3. Limitations of isotropic diffusion model

In **Fig.9**, the experimental results are compared to the results predicted by the isotropic diffusion theory, using Eq. (10), and the FE model presented in Paragraph 4, implementing isotropic diffusivities: $D_Z = D_R = 4.81\ 10^{-8}$ mm^2/s. Note that using the isotropic Eq. (5) would also give the same results for long rods, while axial diffusion is negligible. Isotropic diffusion theory shows good agreement with experimental results for long rods (30 to 300 mm), but underestimates the moisture absorbed by shorter rods (3 and 6 mm long rods).

Fig.9 Weight gain curves for the conditioned samples compared with analytical and FE results obtained using isotropic diffusivity

Results in **Fig.8** and **Fig.9** show that anisotropic diffusion analysis captures very well the faster weight gain for shorter samples, whereas the isotropic diffusion analysis does not.

The analytical anisotropic model has the advantage of simplicity, while the numerical anisotropic model has the advantage of being able to deal with any geometry, boundary conditions and combination of different materials.

The determination of axial and radial diffusivities in CFRP rods can be done both analytically and numerically. The experimental procedure described here requires minimum specimen preparation time, because no sealing of surfaces is needed. The weight measurements are also easily and quickly done. The total measurement period of 70 days was sufficient to obtain the saturation level of the moisture on the short 3 mm specimens. However, a proper calculation of the radial diffusivity could not be done on just the short specimens. Longer specimens are needed, but it is not required to wait until these specimens have reached saturation.

The results showed that the water uptake in the long rods is dominated by radial diffusion, because the additional water absorption through axial diffusion through the ends is minimal. This effect allows simple identification of radial diffusivity. However, it is not clear initially how long a rod has to be to make axial diffusion negligible. Radial diffusivity should always be measured on rods of at least two lengths. If the results of both rods are the same, axial diffusivity can be neglected for these lengths.

Once the radial diffusivity is known, it is possible to obtain axial diffusivity for shorter rods, where diffusion is dominated by axial diffusivity. For the carbon-fiber vinylester rods, it was found that $D_Z = 14.3\ D_R$. The anisotropy factor is high. This effect can be attributed to interphase degradation, as reported by Ramirez et al. [21] for carbon vinylester composites. Looking at **Fig. 3** and **4**, interface degradation also seems to be a reasonable explanation for a rapid diffusion path along the fibers in the rods studied here. An open question is whether the interface is already weak on dry samples, but not visible under the microscope, or if the interface degrades during water uptake. The interface degradation during water uptake would

not be a pure diffusion process. However, the water absorption data indicate Fick behavior. This aspect should be studied in more detail, since it may also be linked to degradation of mechanical properties due to water uptake. It may be the case that materials with low axial diffusivity have better fiber/matrix interface properties.

The testing and the example calculation showed that anisotropic diffusion is not important for predicting the moisture concentration profile of the main body of a pultruded rod. The radial through thickness diffusion governs the water uptake. The same would be true for composite pipes, ship hulls etc. Anisotropic diffusivity becomes important near open edges of a material, leading to a more rapid uptake of water, if the axial diffusivity is higher than the radial diffusivity.

6. Application – Case study of a tether end termination

A case study is reported here, in order to demostrate an industrial application of anisotropic moisture diffusion modelling in composites for the offshore industry.

For composite tethers, umbilicals or any application, the end terminations are a very critical aspect for the design. An axial load applied to the system has to be transferred by radial-axial shear from the rod to the end fitting. Since the radial-axial shear strength of the rods is much less than the axial strength, the load has to be distributed over a large area. For this reason end fittings have to be long. Stress concentrations can also easily develop at transition points and the designer has to find a geometry to keep the stress concentrations to a minimum.

When evaluationg the load bearing capacity of the end fitting, designers evaluate two cases: dry and wet material properties [9]. Usually wet material properties are lower and dominate the design case. However, due to the large length of end fittings, the material inside the end fitting may never get wet. Designing for the wet case may be too conservative.

In order to optimize the design of end fittings it is important to understand to which extend the moisture diffuses into the end fitting during the lifetime of the component. This is done here by means of anisotropic diffusion FE analyses, simulating 5, 10, 25 and 50 years of water exposure.

Fig. 10 (a) shows the geometry of a simplified end fitting of a single CFRP rod in a composite tether. The connection between the rod and end fitting is created by a potting resin, usually a filled polymer. Real end fittings will differ for each producer and the geometry is more complicated than a simple cylinder shown here. Typically several CFRP rods converge together in the metallic casing, where potting resin provides the connection. The aim of this work is to provide a method to find the water concentration in the end fitting that can be extended to any geometry and material. The mechanical design of the end fitting is outside the scope of this work. Therefore, studying a general simplified geometry is sufficient.

A rod length of 150 mm is modelled. 100 mm are covered inside the metallic end fitting. The rod diameter is 6 mm.

By applying specific boundary conditions, shown in **Fig.10 (b)**, it is possible to model only a small part of the rod length, that is hundreds or thousands of meter long in the reality. For an infinitely long rod, axial diffusion is negligible compared to radial diffusivity, however this assumption isn't valid for the end termination. The end fitting is designed as a metallic 100 mm long cylindrical cup having an internal diameter of 8 mm. The space between the rod and the end termination is filled with potting material, typically silicia filled epoxy or filled polyester.

Fig.10 Case study of end termination. The top part is connected to a metal structure, e.g the platform and the bottom part is pultruded rod. In (a) the model and dimensions are shown, in (b) the boundary conditions. Blue filled arrows indicate exposure to water, open white arrows indicate dry conditions.

Water diffusivity in metals is negligible and is described by imposing a zero mass flow boundary condition on the metal´s external surface.

Water exposure is simulated by applying an initial boundary condition of water exposure on the external surface of the rod and potting resin in the uncovered part, shown by a blue line in **Fig.10 (b)**.

In order to account for the purely radial diffusion occuring far from the end termination, zero axial flow is imposed on the bottom and top of the rod. Water diffuses radially into the rod from the outer surface. Near the endfitting some water diffuses axially into the end fitting, creating a combined radial-axial flow. The simulations were checked that the radial flow at the end of the free rod (50 mm away from the end fitting) is not affected by the combined radial-axial flow effect. This was done by also carring out a simulations with a 100 mm long rod and no differnce could be found in the results.

The aim of the analysis is to understand up to which distance the moisture will penetrate into the CFRP rod into the end fitting during the operational life of the tether; here the rod`s diffusivity in the axial direction plays a significant role.

Four-node linear axisymmetric heat transfer quadrilateral elements (DCAX4) having dimensions of 0.1 mm x 0.1 mm were used for the simulation. The mesh is shown in **Fig. 11**. The saturation moisture content was set to 1.4%, as measured for the rods. The radial and axial diffusivities of the CFRP rod were 4.81 10^{-8} mm^2/s and 6.90 10^{-7} mm^2/s respectively, as computed in in the results section.

The potting resin in the end fitting can be made of different materials, therefore different diffusivities are possible. In this study three different values of potting resin diffusivity are analyzed, in order to investigate a wide range of possible behaviours: 1.39 10^{-6} mm^2/s (5 10^{-3} mm^2/h), 1.39 10^{-7} mm^2/s (5 10^{-4} mm^2/h) and 1.39 10^{-8} mm^2/s (5 10^{-5} mm^2/h). The first

diffusivity is a typical value for epoxies or similar materials. The second value, a factor 10 lower, it is typical for composites or lightly filled materials. The last value could be a polymer filled with a very high content of low or zero diffusivity filler material. The potting resin's saturation moisture content was set to 1.5 %.

All the material properties described here refer to 60 °C in distilled water. The diffusivities would be considerably lower at room temperature or in cold water. The effect of temperatures is not investigated here, as the focus of this section is to show how to implement the anisotropic diffusion FE model for a case of general offshore interest, without any particular operational temperature in mind.

Fig.11 FE model of CFRP end termination in epoxy resin. Element size is 0.1 mm

Fig.12 shows the moisture profile along the rod after 5, 10, 25 and 50 years of simulated water exposure. In particular **Fig.12 (a)** shows the moisture profile in case of high potting resing diffusivity, 1.39 10^{-6} mm^2/s, **Fig.12 (b)** in case of medium potting resing diffusivity, 1.39 10^{-7} mm^2/s and **Fig.12 (c)** in case of low potting resing diffusivity, 1.39 10^{-8} mm^2/s.

Fig.12 FE results of moisture content in the axis of the rod after 5, 10, 25 and 50 years of exposure. In grey are reported the results of the isotropic model and in black the results of the anisotropic model: (a) Potting resin diffusivity 1.39 10^{-6} mm^2/s, (b) 1.39 10^{-7} mm^2/s, (c) 1.39 10^{-8} mm^2/s

Complete saturation of the rod inside the end fitting does not occur, even for very long live times (50 years); while the initial 10 mm of rod inside the end fitting are close to saturation from the beginning of operational life (5 years).

The simulated concentration curves in **Fig 12** show that for low diffusivity potting resin approx. 25 mm inside the end fitting the rod's moisture content is higher than 0.5 %; while approx. 70 mm inside the end fitting, the moisture content is null.

For high diffusivity potting resin approx. 50 mm inside the end fitting the rod's moisture content is higher than 0.5 %; while approx. 100 mm inside the end fitting, the moisture content is still not null, 0.2%.

For high diffusivity potting resin, the global diffusion behavior of the end termination is dominated by the diffusivity of the resin, making the concentration profile prediction obtained from the isotropic and anisotropic diffusion models similar. For the potting resin having low diffusivity the concentration profile prediction is dominated by the axial diffusivity of the CFRP rod, making the isotropic model underestimate the penetration length of water compared to the anisotropic model.

This analysis gives useful suggestions for the choice of materials for the potting resin and for the strength assessment of the end termination.

The case study of calculating water concentration profiles in the rod inside a metal end fitting is an example where anisotropic diffusivity is important. If the cylindrical surface of the pultruded rod is sealed by a water impermeable end fitting and potting resin, water can only enter the rod by axial diffusion. In the case studied here the high axial diffusivity allowed the water to penetrate into the end fitting by 75 mm, where it had a very small but visible concentration, see **Fig. 12**. Using the radial diffusivity for calculating the moisture

concentration profile would have given a penetration depth of only 30 mm. On the other hand, if the potting resin has a high diffusivity opening up an axial pathway for the water the entire rod inside the end fitting would see some moisture. The difference between calculating the moisture profile by only the radial or the anisotropic diffusivity becomes less important. In all cases the anisotropic approach predicts a higher moisture content in the end fitting. Typically, the load bearing capacity of the end fitting is dependent on the moisture dependent through thickness shear strength. The example shows that a large part of the end fitting can remain dry even after 50 years, or at least absorb only minimal moisture. This is a good indication that designing end fittings based on properties of saturated materials may be too conservative and a more optimized approach should take moisture dependent properties into account. The optimized approach would require a proper moisture concentration profile inside the end fitting, which can only be obtained taking account of anisotropic diffusivity. Calculating moisture profiles using only radial/isotropic diffusivities would predict too little moisture and could lead to an over-prediction of the load bearing capacity of the end fitting.

7. Conclusions

Anisotropic diffusion characteristics of pultruded carbon fiber rods were obtained by simple weight uptake measurements vs. time. The weight increase of rods of different length was measured and diffusivity in axial (fiber) direction and radial direction could be back calculated. The experimental method is simple, because no surfaces need to be sealed.

The diffusivity in the axial direction was 14.3 times the diffusivity in the radial direction, $6.90\ 10^{-7}$ mm^2/s and $4.81\ 10^{-8}$ mm^2/s respectively. The mass of the rods increased by 1.4% due to water uptake at saturation.

The diffusivities can be obtained from an analytical formula that was derived from Fick´s law for a cylinder considering anisotropy. The radial diffusivity is found first from measurements on long rods, as their behavior is dominated by radial diffusion. The axial diffusivity can then be found from measurements on short rods.

As an alternative, the diffusivities can also be obtained by modeling the rods with a finite element analysis. The results for the analytical and finite element method were basically the same.

Using the well-known approach to calculate diffusivity for isotropic cylinders gives about the same value as for radial diffusivity if measured on long rods. Short rods, where axial diffusivity speeds up the water uptake, can only be analyzed by the anisotropic approach.

The reason for the much higher axial diffusivity is likely a rapid diffusion path through a weak/debonded interface between fibers and matrix. It may be the case that materials with low axial diffusivity have better fiber/matrix interface properties.

The significance of anisotropic diffusivity was shown in an example of a single rod being embedded in a cylindrical metal end fitting. The water concentrations profiles inside the rod were calculated by finite element analysis. If the potting resin keeping the rod in place has low diffusivity water penetrates into the end fitting by about 30 mm based on a calculation using radial diffusivity only. If the higher axial diffusivity is accounted for, the water penetrates about 75 mm into the end fitting. If the potting resin has a high diffusivity it opens an extra axial path for the water penetration outside the rods and the difference between calculations based on radial diffusivity or anisotropic diffusivity become less severe. Optimized strength calculations of rods inside end fittings using moisture dependent properties should always be based on anisotropic moisture profile calculations.

Acknowledgements

This work is part of the DNV GL led Joint Industry Project "Affordable Composites" with nine industrial partners and the Norwegian University of Science and Technology (NTNU). The authors would like to express their thanks for the financial support by The Research Council of Norway (Project 245606/E30 in the Petromaks 2 programme). The authors are also thankful to Carl-Magnus Midtbø and Børge Holen for the realization of the conditioning setup and Eddy Coron and Anton Akulichev for the help with part of the experimental measurements.

References

1. Salama, M.M., et al., *The First Offshore Field Installation for a Composite Riser Joint*. Offshore Technology Conference.
2. Echtermeyer, A.T., *Integrating Durability in Marine Composite Certification*, in *Durability of Composites in a Marine Environment*, P. Davies, Rajapakse Yapa D.S., Editor. 2014, Springer Netherlands: Amsterdam. p. 179-194.
3. Gustafson, C.-G. and A. Echtermeyer, *Long-term properties of carbon fibre composite tethers.* International Journal of Fatigue, 2006. **28**(10): p. 1353-1362.
4. Steuten, B. and M.v. Onna, *Reduce Project and Life Cycle Cost with TCP Flowline*. Offshore Technology Conference.
5. Tavner, C., *Integrated Downline Deployment Package for Efficient Well Intervention*, in *11th Annual Deepwater Intervention Forum*. 2015: Galveston, Texas, USA.
6. Brown, T., *The Impact of Composites on Future Deepwater Riser Configurations*, in *MCE Deepwater Development Conference*. 2017: Amsterdam.
7. Echtermeyer, A.T., Sund, O.E., Ronold, K.O., Moslemian, R, Hassel, P.A.,, *A new Recommended Practice for Thermoplastic Composite Pipes*, in *21st International Conference on Composite Materials*. 2017: Xi'an.
8. *Carbon fiber rods increase umbilical strength without adding weight*, in *Offshore Magazine*. 2008.
9. *DNV-OS-C501, DNV Offshore Standard "Composite Components" Rev.03*. 2013.
10. Springer, G., *Environmental Effects on Composite Materials*. Vol. 1. 1984: Technomic Publishing Company.
11. Springer, G., *Environmental Effects on Composite Materials*. Vol. 2. 1984: CRC Press.
12. Abhilash, A.S., et al., *Micromechanics of diffusion-induced damage evolution in reinforced polymers.* Composites Science and Technology, 2011. **71**(3): p. 333-342.
13. Barjasteh, E. and S.R. Nutt, *Moisture absorption of unidirectional hybrid composites.* Composites Part A: Applied Science and Manufacturing, 2012. **43**(1): p. 158-164.

14. Woo, M. and M.R. Piggott, *WATER ABSORPTION OF RESINS AND COMPOSITES: IV. WATER TRANSPORT IN FIBER REINFORCED PLASTICS.* Journal of Composites Technology and Research, 1988. **10**(1): p. 20-24.
15. Joliff, Y., L. Belec, and J.F. Chailan, *Modified water diffusion kinetics in an unidirectional glass/fibre composite due to the interphase area: Experimental, analytical and numerical approach.* Composite Structures, 2013. **97**: p. 296-303.
16. Joliff, Y., et al., *Study of the moisture/stress effects on glass fibre/epoxy composite and the impact of the interphase area.* Composite Structures, 2014. **108**: p. 876-885.
17. Mallarino, S., J.F. Chailan, and J.L. Vernet, *Interphase investigation in glass fibre composites by micro-thermal analysis.* Composites Part A, 2005. **36**(9): p. 1300-1306.
18. Rocha, I.B.C.M., et al., *Combined experimental/numerical investigation of directional moisture diffusion in glass/epoxy composites.* Composites Science and Technology, 2017. **151**: p. 16-24.
19. Gagani, A., Fan Y., Muliana, A.H., Echtermeyer, A.T., *Micromechanical modeling of anisotropic water diffusion in glass fiber epoxy reinforced composites.* Manuscript submitted for publication, 2017.
20. Storhaug, T., Echtermeyer A. T., Sund, O. E., Salama, M. M., Paulshus, B. *Composite Tethers – Qualified for Ultra Deep Waters*. in *14th International Deep Offshore Technology Conference (DOT 2002)*. 2002. New Orleans, USA.
21. Ramirez, F.A., L.A. Carlsson, and B.A. Acha, *Evaluation of water degradation of vinylester and epoxy matrix composites by single fiber and composite tests.* Journal of Materials Science, 2008. **43**(15): p. 5230-5242.
22. *Standard Test Method for Moisture Absorption Properties and Equilibrium Conditioning of Polymer Matrix Composite Materials*. 2014, ASTM International.
23. La Scala, J.J., et al., *Composites based on bimodal vinyl ester resins with low hazardous air pollutant contents.* Composites Science and Technology, 2008. **68**(7): p. 1869-1876.
24. M. Dawson, P.D., P. Harper, S. Wilkinson, *Effects of conditioning parameters and test environment on composite materials for marine applications*, in *Durability of Composites in a Marine Environment - 2nd Ifremer - ONR Workshop*. 2016: Brest.
25. Fick, A., *Ueber Diffusion.* Annalen der Physik, 1855. **170**(1): p. 59-86.
26. Crank, J., *The mathematics of diffusion*. 1956, Oxford: Clarendon Press.
27. Watson, E.B., K.H. Wanser, and K.A. Farley, *Anisotropic diffusion in a finite cylinder, with geochemical applications.* Geochimica et Cosmochimica Acta, 2010. **74**(2): p. 614-633.
28. Figliolini, A.M. and L.A. Carlsson, *Mechanical properties of carbon fiber/vinylester composites exposed to marine environments.* Polymer Composites, 2014. **35**(8): p. 1559-1569.

Figures

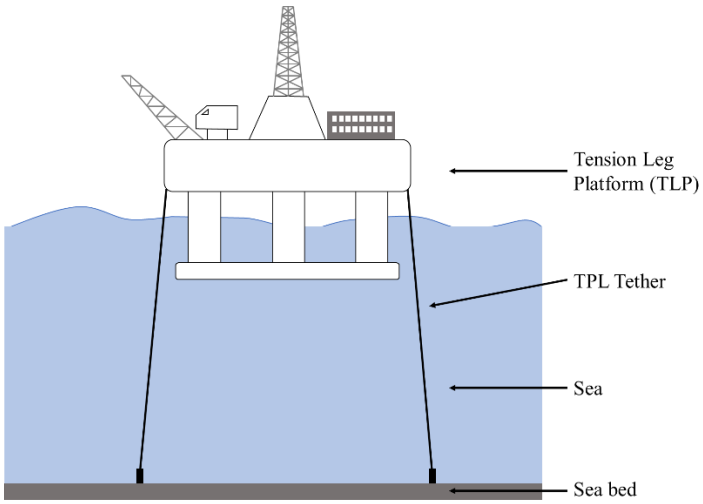

Fig.1 Scheme of a tension leg platform (TLP)

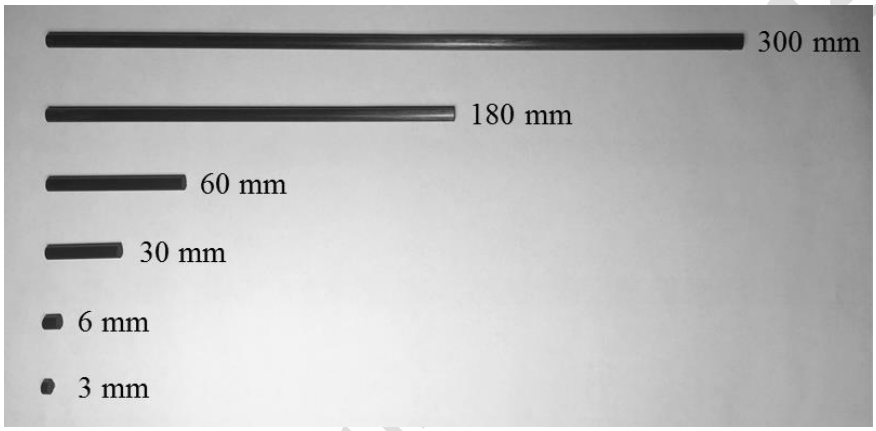

Fig.2 Tested CFRP rods. The diameter is 6 mm the lengths are 3, 6, 30, 60, 180 and 300 mm

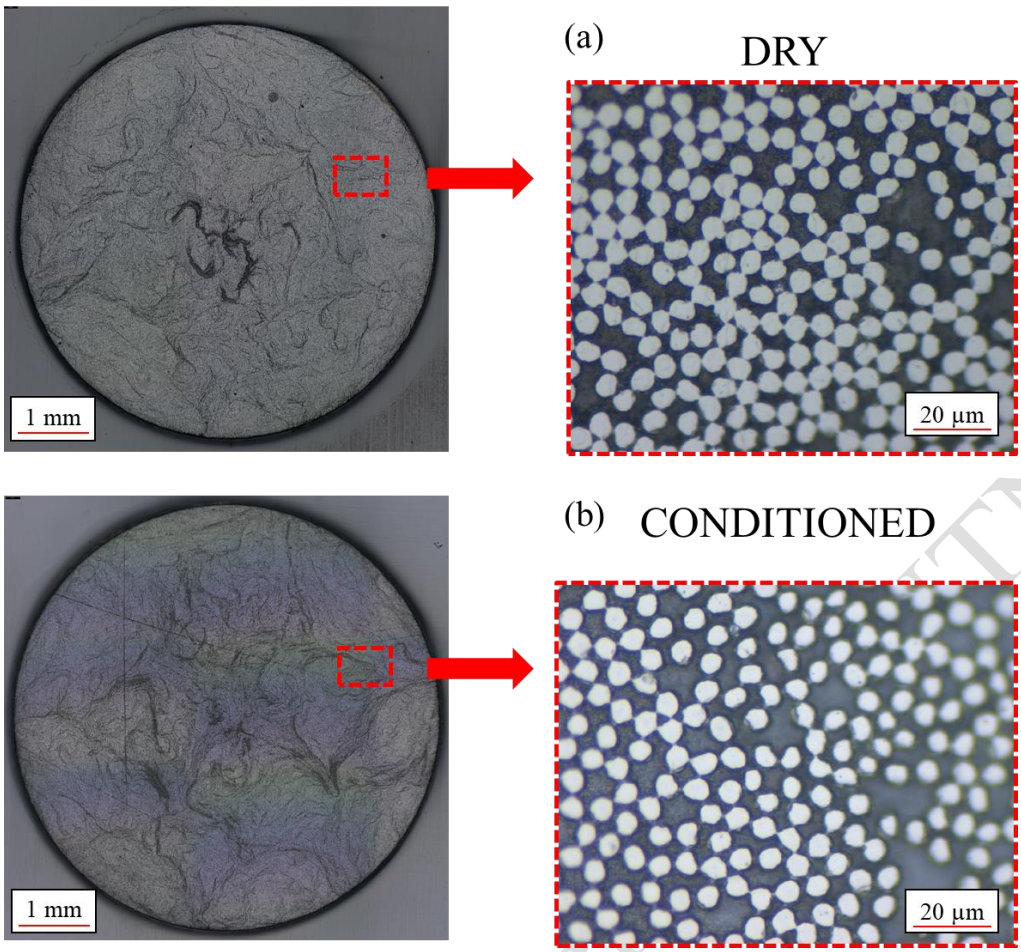

Fig.3 (a) Optical micrographs of dry CFRP pultruded rod. There is no visible damage in the interphase between matrix and fibers. (b) Optical micrographs of conditioned CFRP pultruded rod. Extensive damage is visible in the interphase between matrix and fibers

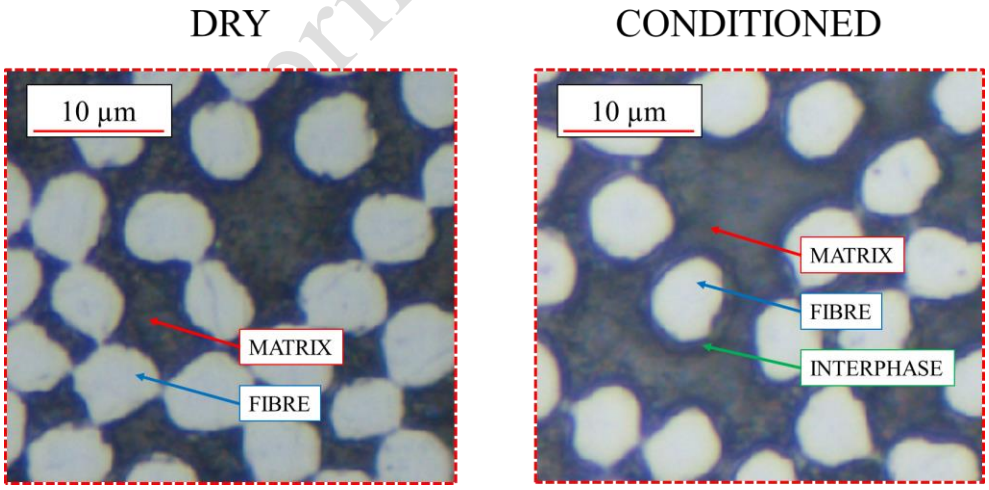

Fig.4 High magnification optical micrographs of dry and conditioned CFRP pultruded rod. Degradation in the 0.4 - 1 µm thick fiber-matrix interphase is visible

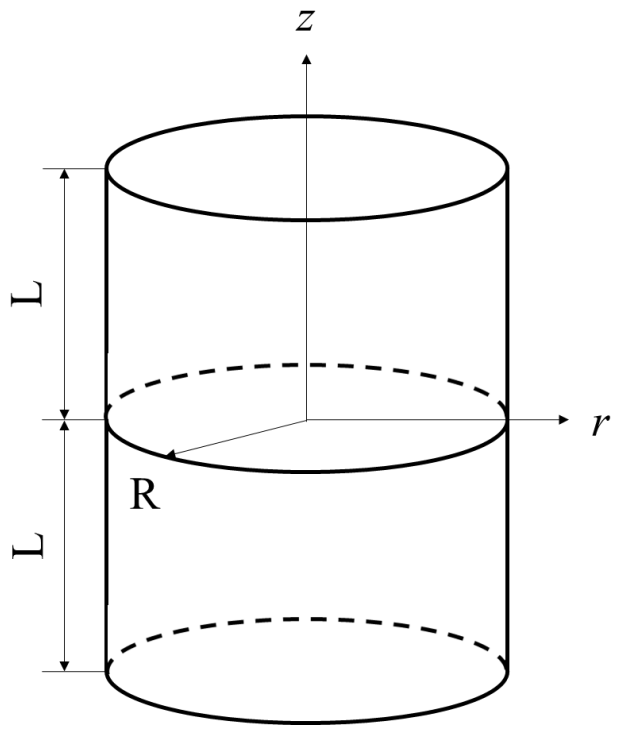

Fig.5 Cylindrical coordinate system and dimensions for anisotropic cylinders

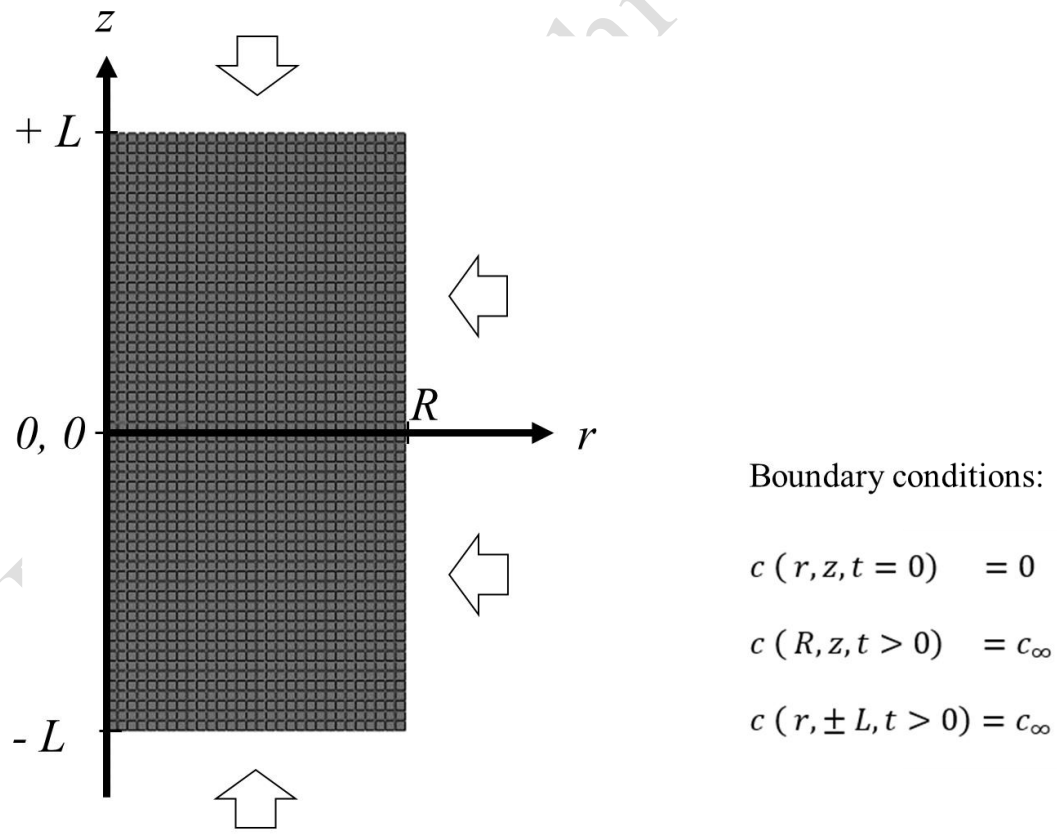

Fig.6 Coordinate system, dimensions and mesh adopted for the 6 mm long rod FE model. Arrows indicate the surfaces exposed to water. Coordinate system and boundary conditions 'equations are also reported.

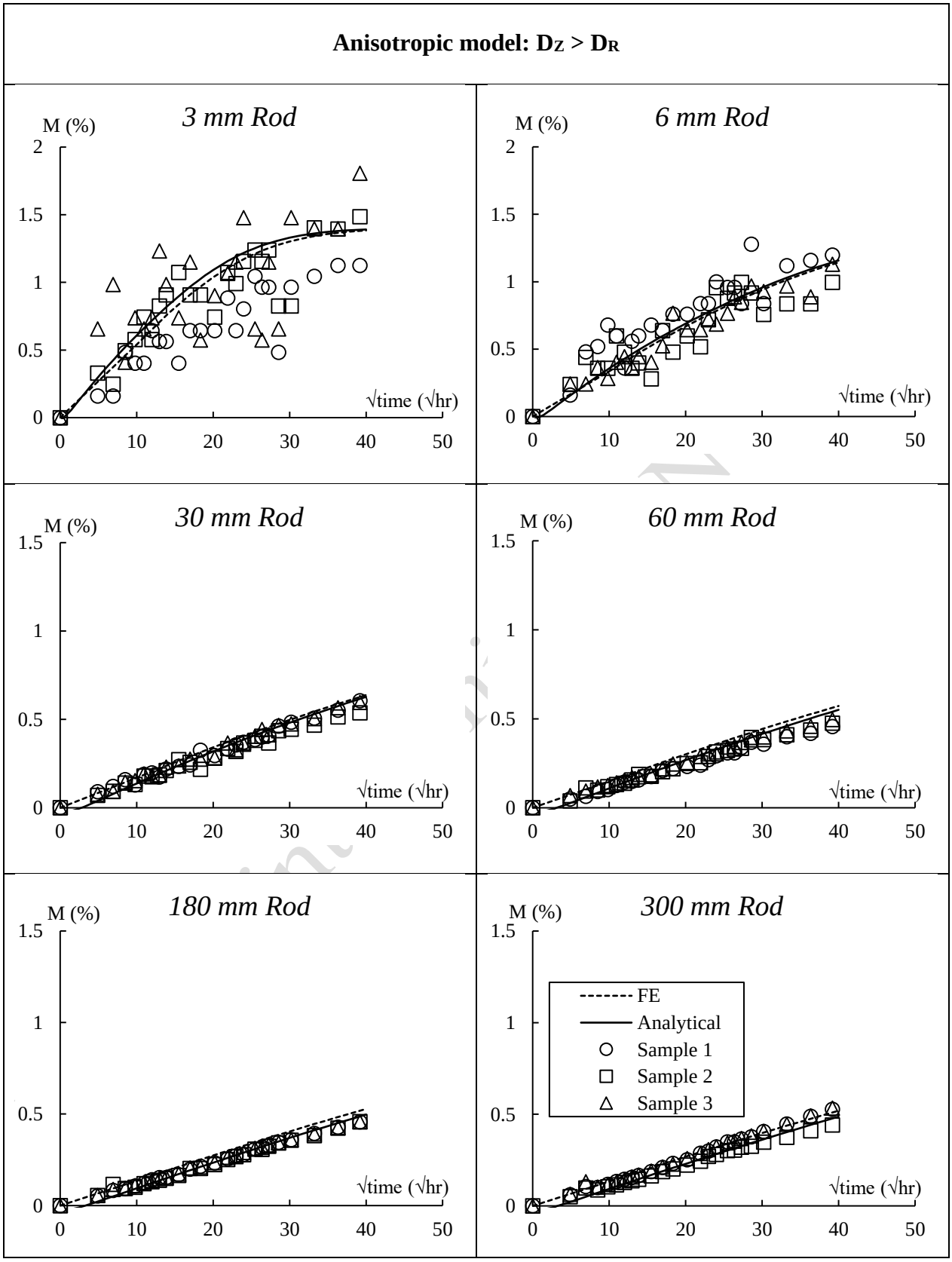

Fig.7 Weight gain curves for the conditioned samples compared with analytical and FE results obtained using anisotropic diffusion constants

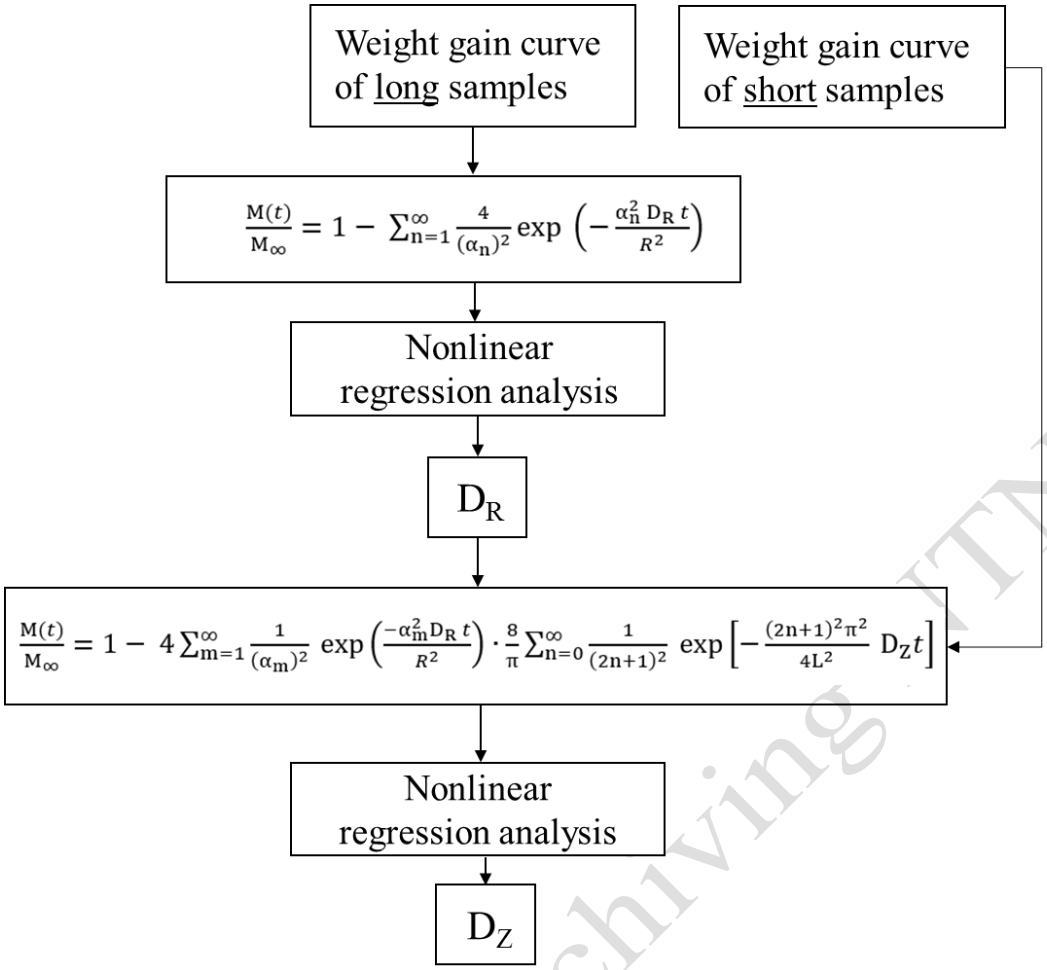

Fig.8 Flowchart for the identification of radial and axial diffusion constants

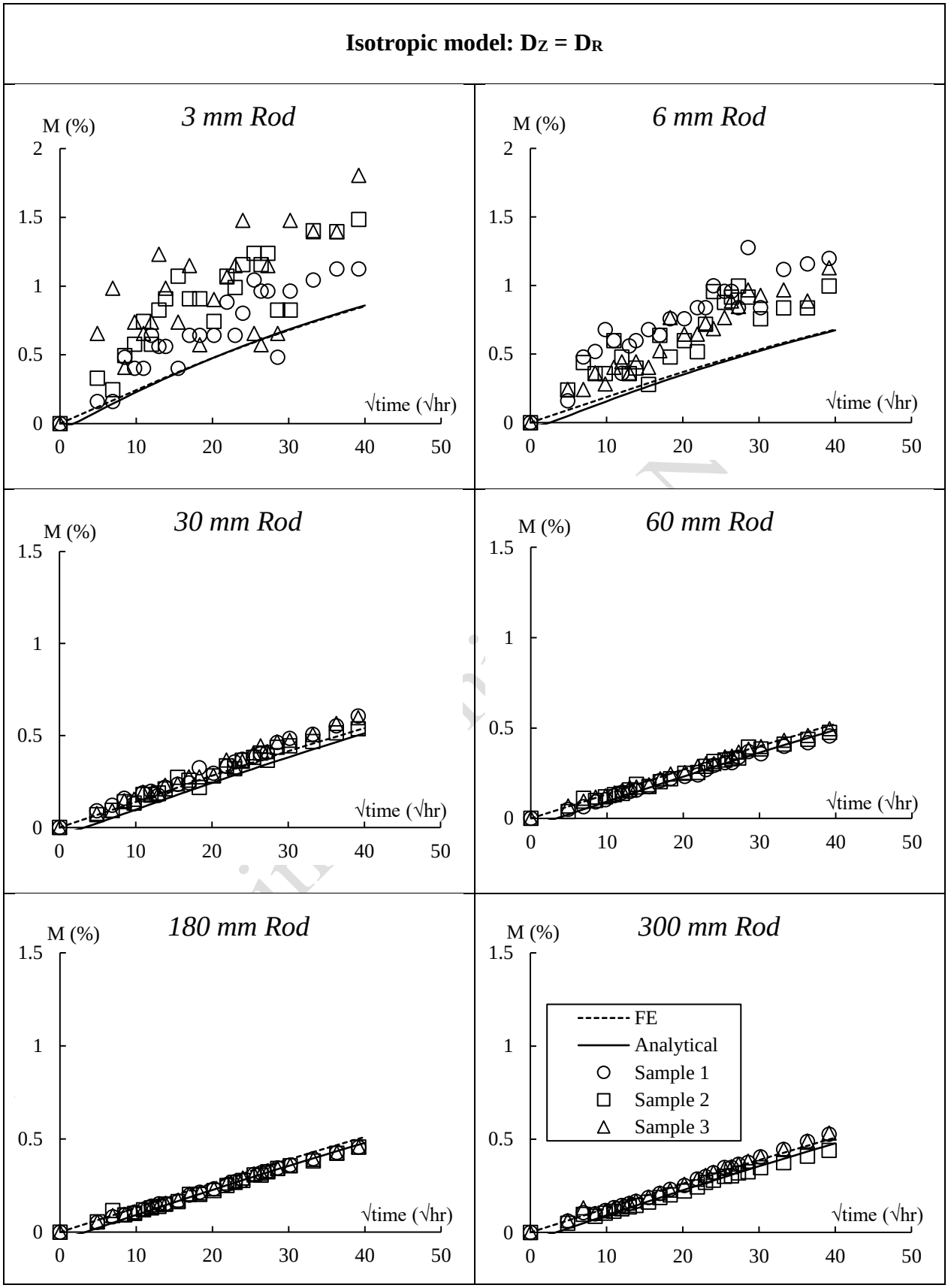

Fig.9 Weight gain curves for the conditioned samples compared with analytical and FE results obtained using isotropic diffusion constants

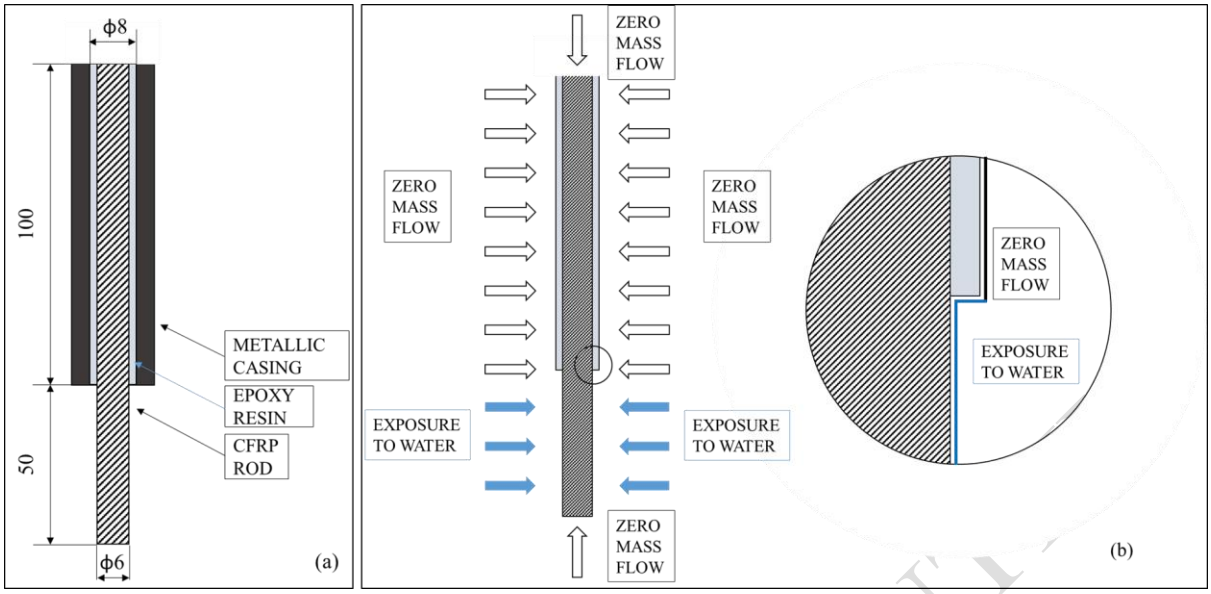

Fig.10 Case study of end termination. Top part is connected to the platform and bottom part is connected to the sea-bed (a) model and dimensions, (b) boundary conditions

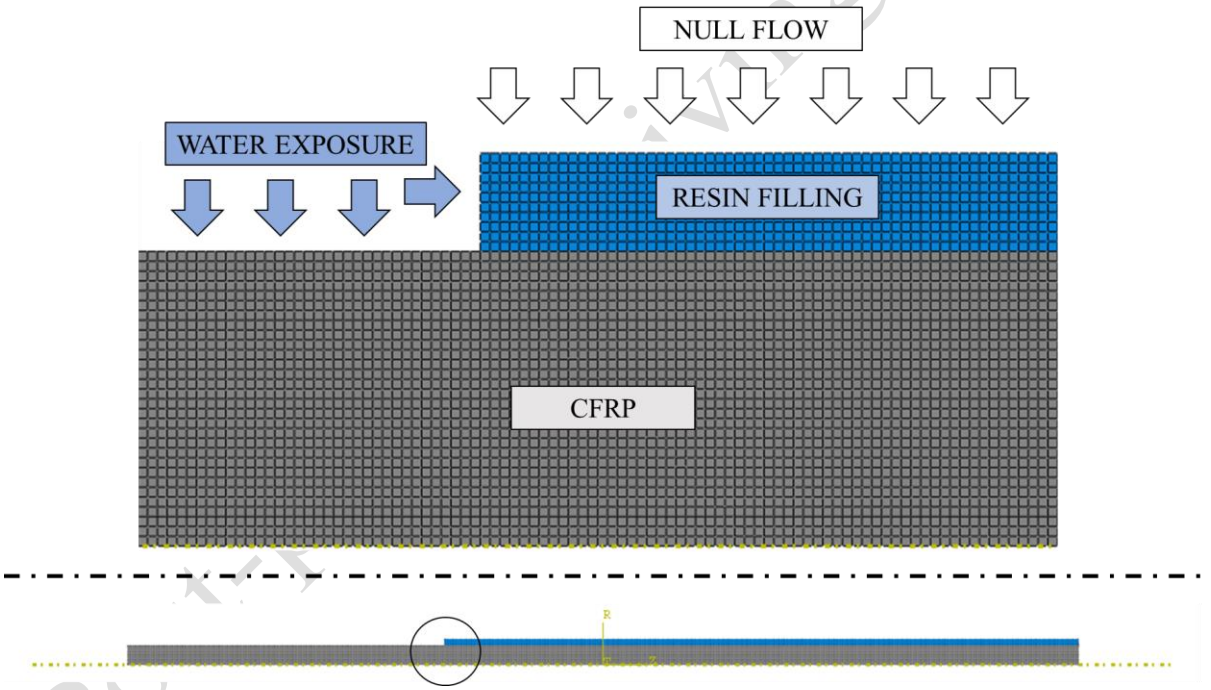

Fig.11 FE model of CFRP end termination in epoxy resin. Element size is 0.1 mm

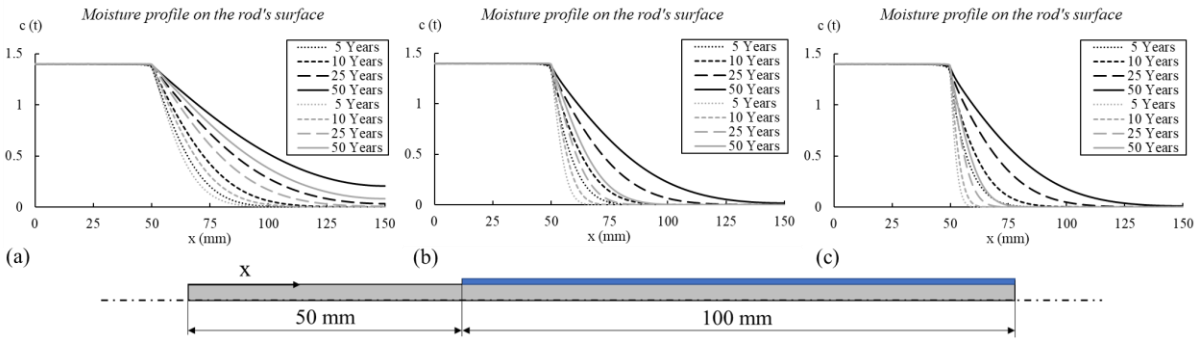

Fig.12 FE results of moisture content in the axis of the rod after 5, 10, 25 and 50 years of exposure. In grey are reported the results of the isotropic model and in black the results of the anisotropic model: (a) Potting resin diffusion constant 1.39 10^{-6} mm^2/s, (b) 1.39 10^{-7} mm^2/s, (c) 1.39 10^{-8} mm^2/s

Tables

Table1: Coefficients of determination describing the quality of the model calculations.

L [mm]	R^2
3	0.8827
6	0.9742
30	0.9969
60	0.9956
180	0.9986
300	0.9960